WELDING RESEARCH

SUPPLEMENT TO THE *WELDING JOURNAL*, JULY 1991

Sponsored by the American Welding Society and the Welding Research Council

All papers published in the *Welding Journal's* Welding Research Supplement undergo Peer Review before publication for: 1) originality of the contribution; 2) technical value to the welding community; 3) prior publication of the material being reviewed; 4) proper credit to others working in the same area; and 5) justification of the conclusions, based on the work performed.

The names of the more than 170 individuals serving on the AWS Peer Review Panel are published periodically. All are experts in specific technical areas, and all are volunteers in the program.

Measurement of Energy Deposition during Pulsed Laser Welding

Energy measuring devices rapidly determine melt depth and eliminate time-consuming cross-sectioning

BY D. A. CREMERS, G. K. LEWIS AND D. R. KORZEKWA

ABSTRACT. The energy deposited in small metal samples by Nd:YAG laser welding pulses (7.8 ms, 36 J/pulse max) was measured using an interferometer and a linear variable differential transformer (LVDT). These devices measured the expansion of a sample due to heating, which was used to calculate the absorbed laser pulse energy. These methods are simple and rapid compared to other techniques using calorimeters or thermocouples. The observed responses of the interferometer and LVDT compared closely with modeling calculations of heat flow and expansion. The effects of incident power density, surface condition, and atmosphere on energy absorption were investigated. Good correlation between deposited energy and melt depth in both the conduction and keyhole mode was obtained for samples of 1100 aluminum and 316 stainless steel. The results demonstrate these devices are useful to determine rapidly the melt depth without the time-consuming steps involved in metallographic cross-sectioning.

D. A. CREMERS is with the Chemical and Laser Sciences Division and G. K. LEWIS and D. R. KORZEKWA are with the Materials Science and Technology Division, Los Alamos National Laboratory, Los Alamos, N. Mex.

Introduction

The interaction between laser radiation and a metal is a complicated process dependent on many parameters of the laser pulse and the metal (Ref. 1). In laser beam welding, optimum process efficiency (energy to form melt pool/incident energy) is achieved by maximizing the laser energy absorbed in the sample. Development of methods to enhance energy coupling require measurement of either the absorbed energy or the molten pool geometry. Molten pool geometry is determined by metallographic cross-sectioning of the samples. Measurements of energy coupling are usually carried out by determining the heat deposited in a sample via calorimetry or by measuring the temperature rise of the sample with a thermocouple. These techniques, although accurate, do not permit rapid evaluation of a large number of samples because they require sample preparation and may not have sufficient sensitivity. In calorimetric-based measurements with samples having low energy coupling efficiencies, for example, it may be necessary to drop the heated sample into liquid nitrogen to determine the deposited energy via vapor generation. In thermometric-based measurements, the thermocouple is usually bonded to the sample to maximize thermal contact. Measurements of melt depth using metallography are tedious and time-consuming.

KEY WORDS

Pulsed Laser Welding
Energy Deposition
Interferometer
LVDT
Nd:YAG Laser
Measurement
Thermal Expansion
Thermodynamics
Transient Expansion
Melt Depth

A rapid and sensitive method of determining absorbed energy without pre or posthandling of the sample is desirable to evaluate efficiently a large number of energy coupling schemes. Several methods have been developed to measure the thermal expansion of solids to determine thermodynamic properties (Ref. 2). This paper describes the use of two of these, an interferometer and a linear variable differential transformer (LVDT), to mea-

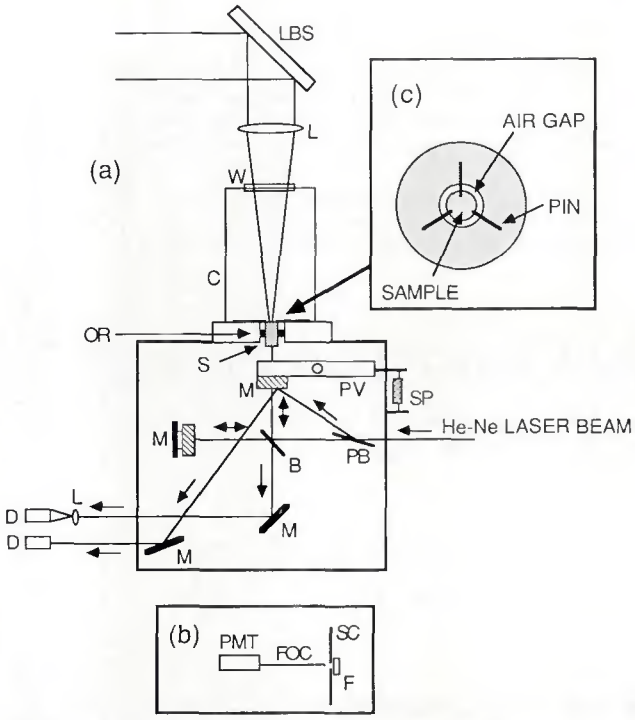

Fig. 1—Diagram of the interferometer used to measure energy deposited in small metal samples. Laser beamsplitter (LBS), lens (L), window (W), chamber (C), sample (S), O-ring (OR), pivoting arm (PV), spring (SP), mirror (M), beamsplitter (B), pellicle beamsplitter (PB), detector assembly (D), fiber-optic cable (FOC), screen (SC), filter (F), and photomultiplier tube (PMT). The detector assembly is shown in (b). The orientation of the sample in the holder viewed from above is shown in (c). The argon purge gas entered the chamber near the sample.

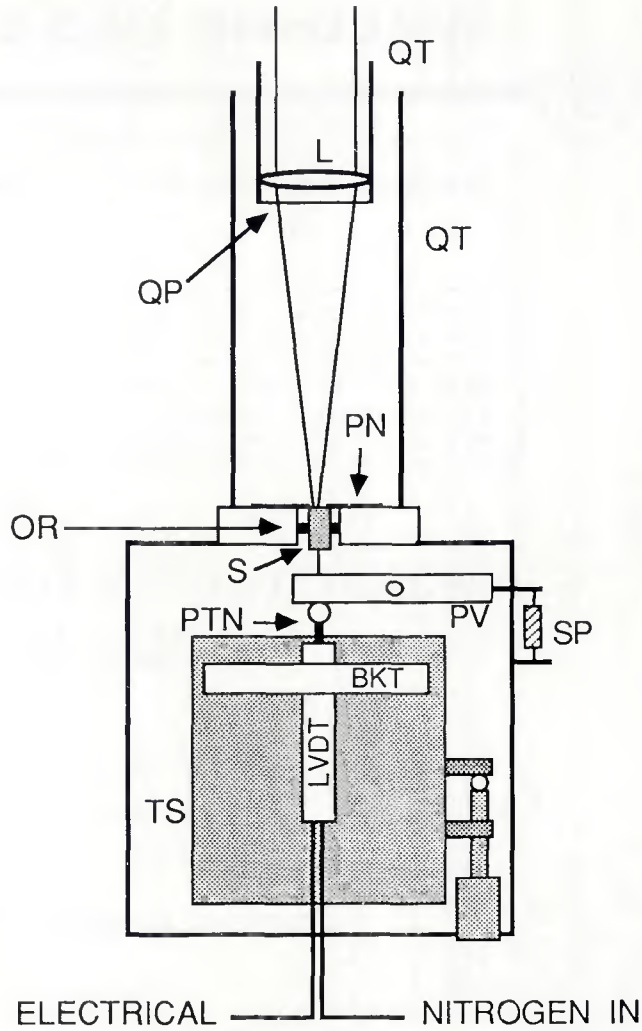

Fig. 2—Diagram of LVDT apparatus. Lens (L), quartz tube (QT), protective quartz plate (QP), steel pin (PN), sample (S), O-ring (OR), pivoting arm (PV), spring (SP), piston (PTN), bracket (BKT) holding LVDT to translation stage (TS). Argon purge gas entered the tube near the sample.

sure the transient expansion of a small sample produced by the absorption of laser pulse energy. The energy deposited in the sample is easily calculated from the expansion. These methods are sensitive and only require physical contact with the heated sample. For example, a simple interferometer can monitor displacements on the order of 1% of the wavelength of light (0.0063 μm for the helium-neon laser) and the LVDT can monitor displacements down to 0.1 μm.

The use of the interferometer and LVDT to measure effects of power density, surface condition, and atmosphere on energy coupling in samples of 1100 aluminum (1100 Al) and 316 stainless steel (316 SS) is demonstrated in this paper.

Experimental

Laser Beam Welding System

The Nd:YAG laser beam welding system used here (Raytheon SS-500) generated pulses with a width of 7.8 ms and a maximum energy of 36 J. In order to stabilize beam characteristics with respect to thermal effects in the cavity, the laser was operated at 10 Hz for five seconds before the shutter was opened to direct a single pulse to the sample. The pulse was focused on the sample by a quartz lens (100-mm focal length, 25.4-mm/1-in. diameter, antireflection coated for 1.06 μm). The pulse energies and power densities listed here were those incident on the sample surface after accounting for all losses.

The focal position and focused spot size of the laser pulses were determined by passing a series of gold wires (0.127-mm/0.005-in. diameter) through the focal plane at high velocity and monitoring the reflected light with a photodiode. This method is described in detail in Ref. 3. The power densities listed here refer to the power within the maximum detectable spot size using this method. No attempt was made to determine the $1/e^2$ size of the focal spot. Although the laser generated spatial modes of higher order than TEM_{00}, the temporally integrated spatial profile of the laser pulse at the sample appeared Gaussian-like as measured using a two-dimensional pyroelectric array.

Because the spatial properties of the pulses depended on energy, the laser was operated at the same near maximum pulse energy setting in all experiments. The energy incident on the sample was changed by inserting beamsplitters having different reflectivities above the sample, as shown in Fig. 1. The focal position and focal spot size were measured for each beamsplitter. The focal position remained fixed, but the spot size changed slightly from 0.81 to 0.86 mm (0.032 to 0.034 in.) using the different beamsplitters. The lens-to-sample distance was adjusted to produce the minimum spot size on the sample.

Interferometer Apparatus

A diagram of the Michelson interferom-

eter used to measure sample expansion is shown in Fig. 1. The metal samples were small solid cylinders (6.35 mm/0.25 in. long by 3.18 mm/0.13 in. diameter). The small size maximized sample expansion due to heating. Unless stated otherwise, the sample surface was used as machined and was cleaned with ethanol prior to use. The top of the sample rested against three steel pins (0.58-mm/0.02-in. diameter) spaced 120 deg apart. The pins contacted the sample only on the outer edge to minimize heat transfer and to provide the largest clear area on which to focus the laser pulse. The top of the sample was held in position against the pins by a spring-loaded pivoting arm that contacted the sample at the bottom through a thin steel pin. The force exerted on the bottom of the sample by the pivoting arm minimized movement of the sample due to pressures generated in the sample during the laser pulse. The laser pulse was incident on the sample from the top as shown in Fig. 1. As the sample heated, it expanded downward rotating the pivoting arm. A mirror was attached to the arm to form one path of the interferometer. The second path of the interferometer was formed by a stationary mirror. The fringe pattern obtained by combining the two beams was expanded by a lens and projected on a screen with a pinhole in the center—Fig. 1b. A fiber-optic cable behind the hole carried the transmitted light to a photomultiplier tube for detection. A filter was placed in front of the screen to block scattered laser radiation from the detector. As the sample expanded due to heating, the mirror pivoted downward changing the optical path length through this path of the interferometer. For the displacements observed here (40 μm maximum), the error introduced by moving the mirror along an arc rather than parallel to the direction of sample expansion was negligible. The fringe shift (F) is related to the change in length (ΔL) of the sample through the equation,

$$F = \Delta L / \lambda_{laser} \qquad (1)$$

where λ_{laser} is the wavelength of the He-Ne laser.

It was not possible to determine easily the direction of the change in sample length (*i.e.*, expansion or contraction) from the fringe shift. This direction was determined by splitting off a portion of the incident He-Ne beam as shown in Fig. 1. This second probe beam was reflected off the pivoting mirror at an angle and the deflection of the beam was monitored using a second pinhole and detector assembly.

The atmosphere above the sample was purged with a gas or gas mixture using the quartz chamber shown in Fig. 1. Unless stated otherwise, all measurements were carried out with a flow of argon at Los Alamos atmospheric pressure through the chamber. A small vent provided an exit for the gas. An O-ring was positioned around the sample to complete the chamber seal.

Samples were loaded into the interferometer by moving the pivoting arm downward and sliding the sample with O-ring up into position. The location of the sample under the pins was observed from above using a microscope and appeared as shown in Fig. 1c. About one minute was required to change a sample. Because the lengths of the samples were slightly different and the samples were not positioned in the device in exactly the same orientation, it was necessary to adjust the interferometer mirrors slightly to align the fringe pattern on the screen over the pinhole.

The signals recorded on each experiment were 1) the laser pulse, 2) the fringe shift at fast- and slow-sweep rates on separate channels of a digital-storage oscilloscope (Nicolet 4094C), and 3) the direction of motion of the pivoting mirror to indicate sample expansion or contraction.

Table 1—Mass and Energy Content of Material Ejected from 1100 Al and 316 SS

Pulse Energy (J)	Material	Avg. Mass Ejected (mg)	Energy Content (J) at Melt. Pt.	Energy Content (J) at Boil. Pt.
28.1	1100 Al	0.5	0.6	1.5
31.5	1100 Al	1.1	1.2	3.4
21.5	316 SS	1.5	1.8	3.7
24.5	316 SS	3.6	4.4	8.8
31.5	316 SS	8.2	10.1	20.1

LVDT Apparatus

The LVDT is a small transformer with movable primary and secondary windings that undergo relative displacements as a central piston is displaced linearly. The position of the piston is determined using an inductance bridge circuit. The LVDT system was a Schaevitz Engineering model LBB-375-TA-100A transducer and model DTR-451 readout. The transducer was mounted vertically on a translation stage as shown in Fig. 2. The piston of the LVDT was pressurized with 10 psi (68.9 kPa) of nitrogen to provide a force of about 4 oz. (113 g) against the pivoting arm, which was spring-loaded to hold the sample in position securely against the retaining pins as described above for the interferometer. The design of the LVDT apparatus required that the samples (9.53-mm/0.37-in. long by 3.18-mm diameter) be 50% longer than those used with the interferometer.

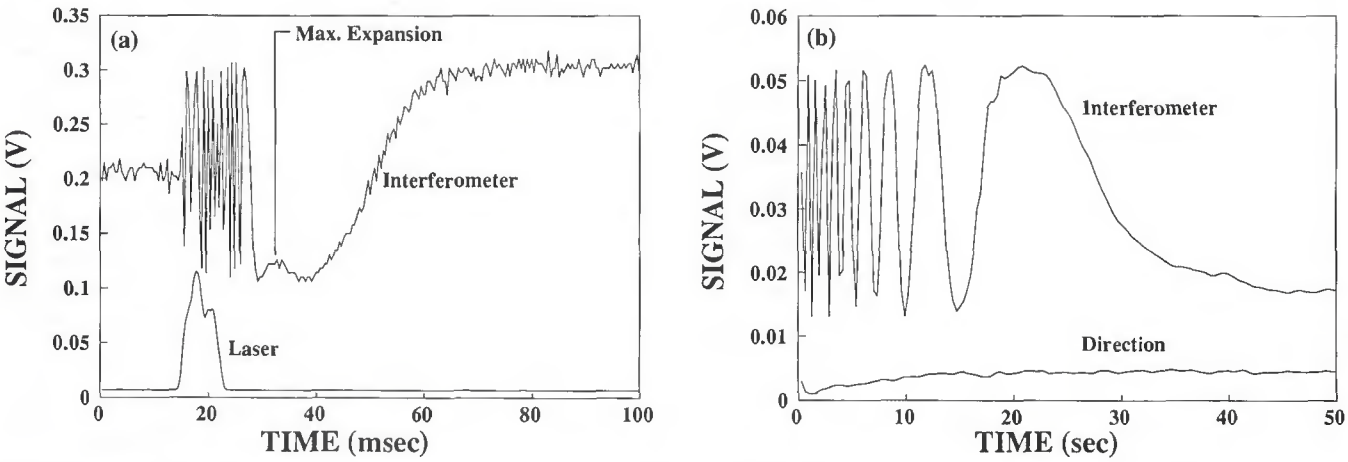

Fig. 3—a—Fringe shift during heating and the laser pulse recorded as 1100 Al was heated by an 18.8-J pulse. b—Fringe shift and the direction of sample expansion/contraction recorded on a slow-time scale to show cool down. Contraction of the sample is indicated by a positive-going signal on the bottom trace of b.

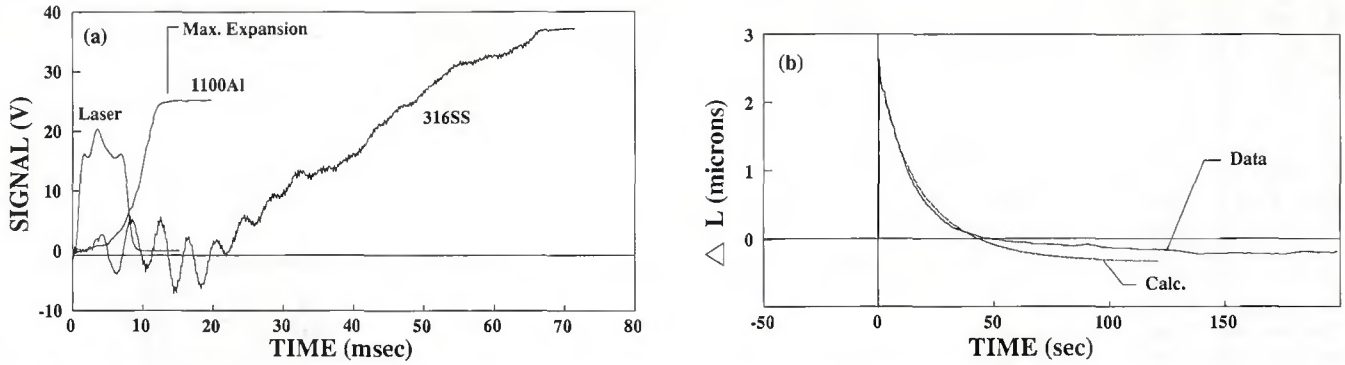

Fig. 4 — a — Signals from the LVDT and a photodiode monitoring the laser pulse as samples of 1100 Al and 316 SS were heated by a 17.3-J laser pulse. b — Calculated and measured signals from the LVDT as the 1100 Al sample cooled.

After loading a sample, the LVDT readout was zeroed by moving the transducer vertically on the translation stage. The readout circuitry was adjusted to maximize sensitivity: an 8-V signal was obtained for a displacement of 0.203 mm. The LVDT response was calibrated using steel shims of known thickness.

The region above the sample was purged with argon using the arrangement of coaxial quartz tubes shown in Fig. 2. A high flow rate of argon was maintained through the chamber to prevent backstreaming of air through the narrow gap between the tubes. The focusing lens was mounted at the end of the inner tube and a quartz plate protected the lens from ejected material.

The signals recorded on each experiment were 1) the laser pulse and 2) the LVDT voltage at fast- and slow-sweep rates on separate channels of a digital-storage oscilloscope.

Evaluation

Calculation of Deposited Energy

The expansion of the sample due to laser heating was computed using the difference between the maximum signal voltage (*i.e.*, maximum expansion) and the voltage measured at long times, when the sample reached room temperature. The easiest method to compute the deposited energy is to assume that 1) the heat lost during expansion was negligible and that 2) the maximum expansion occurred when the heat was distributed uniformly throughout the sample. As demonstrated below, the first criterion was satisfied because the time required for the sample to reach maximum expansion was much less than the time required for complete cool down. The second criterion requires consideration because uniform heat distribution will not necessarily produce maximum expansion. If the specific heat (c_p) and thermal expansion coefficient (α) are independent of temperature, expansion will be the same if the heat is located only in the upper portion of the sample immediately after the laser pulse or if the heat is uniform throughout the sample. In general, however, c_p and α are temperature dependent so the expansions obtained from these two heat distributions will be different. If c_p and α are not strongly temperature dependent, however, this difference will be small.

To compute this difference, the cylindrical sample is divided axially into five disks each one-fifth the total length of the sample. The energy deposited in the top disk by the laser pulse (Q) is given by

$$Q = 0.2M\int c_p(T)dT \qquad (2)$$

where M is the mass of the sample and the integration extends from room temperature (T_o) to T. For a given Q, T can be computed. The temperature of the sample following uniform distribution of the same amount of heat (T′) is computed similarly using

$$Q = M\int c_p(T)dT \qquad (3)$$

The difference in sample expansion obtained in the two cases is computed using

$$\delta L = (\Delta L) - (\Delta L)' = 0.2L_o\int \alpha(T)dT - L_o\int \alpha(T)dT \qquad (4)$$

where the first integral is evaluated from T_o to T and the second integral is evaluated from T_o to T′. Here L_o is the length of the sample before heating. For Q = 8J, T_o = 293 K, T = 695 K, T′ = 337 K (the latter two obtained from Equations 2 and 3), and values of $c_p(T)$ and $\alpha(T)$ from the literature (Refs. 4, 5), the values of (ΔL) and (ΔL)′ for 1100 Al become 10.50 and 10.24 μm, respectively, so that δl = 0.26 μm or the expansion is 2.6% greater when the heat is deposited in the top fifth of the sample. A similar calculation for 316 SS yields a 2% difference. Therefore, for these materials and the experiments described here, it is valid to use the maximum observed expansion to compute deposited energy by assuming uniform heat distribution.

The energy deposited in the sample was computed from the measured expansion (ΔL) by considering the heating process as a series of discrete steps ranging from room temperature (T_o) up to T′, the maximum uniform temperature of the sample produced by absorption of the laser pulse energy. Each step is labeled according to its temperature T_i, where i = 0,1, 2, . . . n. Values for $\alpha(T)$ and $c_p(T)$ at each temperature are computed from the known dependence of these parameters on temperature (Refs. 4, 5).

Let $\alpha(T_o)$ and $c_p(T_o)$ be the linear expansion coefficient and specific heat at T_o. Let $a(T_1)$ and $c_p(T_1)$ be the values of these parameters at the slightly higher temperature of $T_1 = T_o + dT$ produced by adding a small amount of heat dQ_1 to the sample. The value of dQ_1 is given by

$$dQ_1 = dLc_p(T_o)M/[L_o\alpha(T_o)] \qquad (5)$$

where L_o is the original sample length, dL is the incremental sample expansion [ΔL = ndL], and M is the sample mass. The value of dT_1 is given by

$$dT_1 = dQ_1/[c_p(T_o)M] \qquad (6)$$

The energy absorbed during the next incremental expansion is computed using the formula

$$dQ_2 = dLc_p(T_1)M/[L_o\alpha(T_1)] \qquad (7)$$

and the new temperature $T_2 = T_o + dT_1 + dT_2$ is found by calculating dT_2

$$dT_2 = dQ_2/[c_p(T_1)M]. \qquad (8)$$

These calculations proceed through the n incremental expansions until the final temperature T_n = T′ and total energy deposited Q = ΣdQ are reached.

Interferometer Response

Typical signals obtained by heating an 1100 Al sample with a single laser pulse are shown in Fig. 3. The laser pulse and the fringe shift recorded during heating are shown in Fig. 3a. The fringe shift obtained by contraction of the sample during cooling and the signal produced by deflection of the second probe beam are shown in Fig. 3b. The data indicate that expansion begins during the laser pulse and is complete within 18 ms after the start of the pulse. Because of the oscillatory appearance of the fringe shift signal, there is some

uncertainty in choosing the exact time of maximum expansion. For many samples, there was no consistent progression of fringes during heat up useful to measure sample expansion. This could have been due to several factors including 1) nonuniform distribution of heat in the sample during and immediately after the pulse, which may have temporarily distorted the sample; 2) impulse forces generated by the energy deposition process, which moved the sample; and 3) the inertia of the pivoting mirror assembly, which prevented fast response of the interferometer during heat up. For this reason, the fringe shift produced during cool down was used to measure sample expansion. The transition between heating and cooling periods is evident from the change in spacing of the fringes and the direction of motion of the second beam.

An estimate of the relative importance of energy lost during expansion to the total energy deposited in the sample is obtained by computing the ratio of the cooling and heating time periods. From Fig. 3a and b this ratio is (50/0.018) = 2778 for 1100 Al. The data for 316 SS give a ratio of (170/0.150) = 1133. Therefore, heat loss during expansion was minor, validating the assumption made in the calculation of deposited energy.

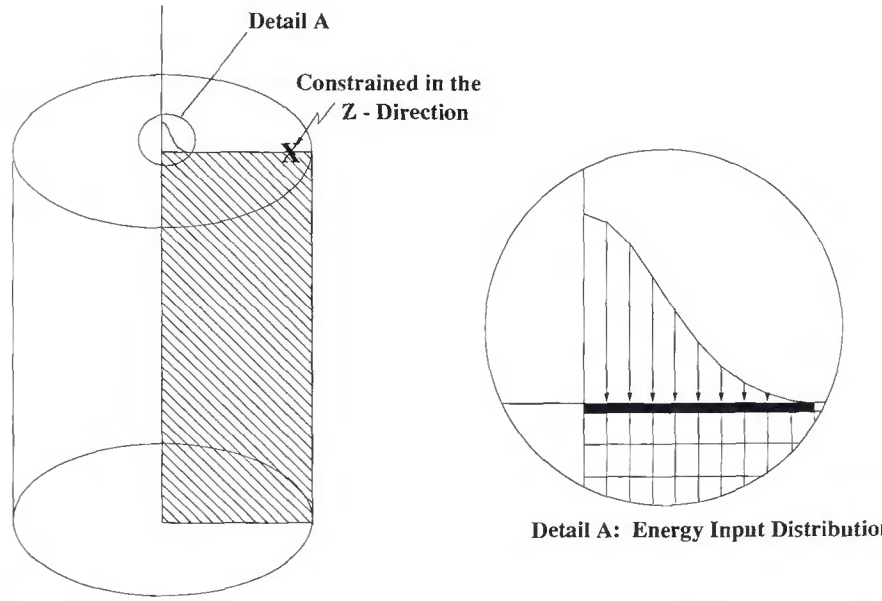

Fig. 5 — Diagram of the plane through the sample used to model heat flow produced by a Gaussian laser pulse incident on one end. The top of the sample was constrained in the z-direction by the steel pins.

The LVDT Response

Typical signals obtained from the LVDT while monitoring the expansion of 1100 Al and 316 SS samples are shown in Fig. 4a along with the laser pulse. The signal recorded during contraction of 1100 Al is shown in Fig. 4b along with results obtained by modeling the expansion/contraction of the sample as described below. Figure 4a shows essentially the same results noted above for 1100 Al with the interferometer: heating begins during the pulse and appears complete within 15 ms. Because of the small sample diameter and the high thermal conductivity of aluminum, expansion of the sample during the pulse would be expected due to diffusion of heat from the melt zone to the outer perimeter.

The heating phase of 316 SS was different from that observed for 1100 Al: there was oscillation of the LVDT signal during the first 30 ms after the start of heating followed by expansion, which reached a maximum at about 170 ms. Oscillations were observed for 316 SS but not for 1100 Al. Their origin was not determined. The longer expansion time for steel is expected because the ratio of the thermal diffusivities of 316 SS and 1100 Al is about 25 at 300 K (Ref. 5).

The experimental conditions used to obtain the data in Figs. 3b and 4b were similar so the cooling times should agree closely. Analysis of the data shows this to be the case. According to Fig. 3b, the fringe shift is complete within about 50 s, whereas Fig. 4b shows that the sample is within about 5 to 7% of room temperature at 50 s. A somewhat slower cool down of the 50% longer LVDT samples would be expected because the ratio of surface area to volume is 94% of that for the interferometer samples. The cooling curve in Fig. 4b also shows that the LVDT piston did not return to the original starting position when the sample reached room temperature. This was observed in many measurements and was probably due to minor displacement of the sample during the laser pulse. The zero offset shown in Fig. 4b, for example, corresponds to a distance of only 0.8 microns. Replicate measurements showed that if the difference between the maximum signal and the LVDT signal at long times was used to compute the change in length due to heating, reproducibilities of 3 to 8% were possible.

Comparison with Modeling Calculations

Numerical modeling of the heat transfer and subsequent expansion of a sample was carried out using the general purpose finite element code ABAQUS (Ref. 6). ABAQUS offers fully coupled, simultaneous heat transfer and expansion analysis. The problem was run using two-dimensional axisymmetric elements with boundary conditions applied to the mesh as shown in Fig. 5. A Gaussian heat distribution was used for the heat source model, applying the heat calculated from the LVDT data. Heat was supplied for the duration of the laser pulse (7.8 ms). Both radiative and convective heat losses were applied to the outer sample surfaces. ABAQUS allows for thermal conductivity, specific heat, and thermal expansion to be temperature dependent. It also applies a heat of fusion and a heat of vaporization over a range of temperatures. The rate of cooling is very dependent on the film coefficient describing convective heat loss through the sample walls. This coefficient is geometry dependent, especially for small specimens and was adjusted here to obtain the best fit.

Isotherms showing the heat distribution in 1100 Al at different times after the start of the laser pulse are shown in Fig. 6. The retaining pins contacted the sample on the top surface within 0.3 mm (0.01 in.) of the edge and because of this expansion is only observed when there is a thermal gradient between the pins and the bottom of the sample. As observed experimentally, the isotherms indicate that expansion begins during the laser pulse. In addition, comparison of the isotherms near the outer top edge at different times shows that the maximum thermal gradient between top and bottom occurs between 10 and 20 ms after the start of the pulse, which agrees with the heating curves of Figs. 3a and 4a. Figure 6 also shows that the heat is distributed uniformly throughout the sample by 0.5 s. Examination of the LVDT signal for 1100 Al during the first few seconds shows that the maximum expansion attained within 20 ms after the start of the laser pulse still exists at 0.5 s because the cooling rate is slow in comparison to heat transport and because of the small change in sample length due to heat redistribution, as calculated above. The experimental and calculated cooling curves compare closely as shown in Fig. 4b for 1100 Al. The ABAQUS results were aligned to the experimental data at the point of maximum expansion so the calculated curve, as the

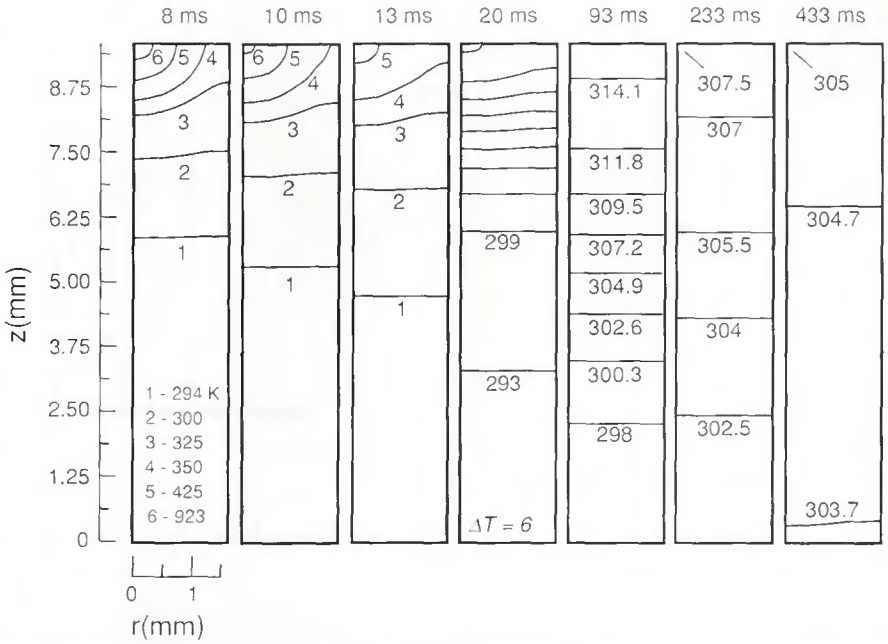

Fig. 6—Isotherms for 1100 Al at different times after the start of a 7.8-ms laser pulse assuming a deposited energy of 8.2 J. The laser pulse was incident on the sample from the top at t = 0. The temperatures for the three plots on the left are listed on the 8-ms plot. The temperature difference between isotherms on the 20-ms plot is 6 K.

experimental data, does not return to zero.

A similar analysis of isotherms for 316 SS (17.3 J/pulse) shows that uniform heat distribution is approached about 10 s after the start of the laser pulse, but the LVDT data shows that by this time the sample has contracted by about 30% of its maximum value. As calculated previously, a small amount of this contraction results from diffusion of heat in the sample to form a uniform distribution but most of it is due to heat loss through convection. The effect of cooling in relation to heat distribution is more pronounced in 316 SS because the thermal diffusivity is about a factor of 25 less than for 1100 Al. About 150 s are required for 316 SS to reach room temperature.

Table 2—Percent Energy Deposition as a Function of Atmosphere and Surface Condition

Surface	Air	Argon
1100 Al (18.8 J/pulse)		
(machined)	27	22
(1-6 micron)	29	23
(120 micron)	32	26
(grit-blasted)	34	33
1100 Al (18.8 J/pulse)		
machined	–	23
black anodized	–	36
0.013 cm hard coat	–	36
0.025 cm hard coat	–	36
Copper (35.4 J/pulse)		
machined	–	5
ebanol-c (light coat)	–	24
ebanol-c (heavy coat)	–	25

Results and Discussion

Ejected Material

At power densities of 0.50 MW/cm^2 (316 SS) and 0.55 MW/cm^2 (1100 Al) and higher, molten material was ejected from the samples by the laser pulse. The ejected mass was determined by weighing the sample before and after each experiment and average values are listed in Table 1 along with calculations of the energy removed by assuming the mass was at the melting and boiling temperatures. These represent lower and upper bounds for the energy content of the ejected material: the material must be molten to be ejected but additional heating and some vaporization occurs during the laser pulse (Ref. 7). Because the laser pulse coupled more efficiently into 316 SS, significantly greater masses were ejected from 316 SS compared to 1100 Al. The greater coupling is due to the lower thermal diffusivity and lower reflectivity of 316 SS compared to 1100 Al.

Measurements of Deposited Energy

The energy deposited in 1100 Al and 316 SS as a function of the incident laser pulse power density is plotted in Fig. 7. Two sets of data are shown in each figure corresponding to the energy deposited in the sample computed from the LVDT signal and the total energy absorbed computed as the sum of the energy from the LVDT signal plus the energy carried away assuming the ejecta was at the melting temperature.

The data for 1100 Al in Fig. 7a show two main features. First, two distinct linear regimes are evident according to power density. The lines shown were fit to the data for each of these regimes. The data corrected for the energy removed by ejected material were used to fit the curve at the highest powers. The slope of the curve for power densities below 0.43 MW/cm^2 is significantly less than the slope at higher power densities. The fraction of incident energy coupled into the sample ranges from about 15% at the lowest power density up to an average of about 44% at the highest power. The dependence of deposited energy on power density found here agrees with previous data for 1100 Al and 304 SS that show an increase in melt depth with increased power density (Ref. 8). The increased coupling efficiency above 0.43 MW/cm^2 may be related to significant melting of the sample: a large decrease in reflectivity has been reported upon laser-induced melting of aluminum (Refs. 9, 10). The second feature is that at a power density of 0.48 MW/cm^2 and above, the scatter in the data increased significantly. At power densities below 0.43 MW/cm^2, the percent relative standard deviation (RSD) of replicate measurements ranged from 3 to 11%, whereas the RSD for data at 0.48-0.49 MW/cm^2 was 36% and remained large at higher power densities. This abrupt increase in the RSD can be explained by examining cross-sections of welds made in 1100 Al at 0.49 MW/cm^2 using identical conditions. Two examples are shown in Fig. 8, which correspond to the maximum and minimum of energy deposited at this power density. At the lowest deposited energy, the weld shape is characteristic of the conduction mode, whereas at the highest deposited energy, the weld shape shows the onset of keyholing (Ref. 11). Interestingly, the melt depths of the eight samples at 0.48–0.49 MW/cm^2 were in the ranges of 0.26 to 0.28 mm or 0.76 to 0.97 mm, with no intermediate values. Therefore, the large RSD can be attributed to operation at a power density corresponding to the threshold for keyholing. The shape of the melt at threshold is apparently sensitive to small differences between replicate experiments such as sample surface condition or laser pulse characteristics. At powers of 0.55 MW/cm^2 and above all welds exhibited the keyhole shape. The large RSD obtained above 0.55 MW/cm^2 can be attributed to ejection of material from the weld pool, errors involved in calculating the energy removed by the ejected mass, and shot-to-shot differences in the dynamics associated with ejection of mass from the melt pool, which would introduce noise into the measurements.

The data for 316 SS in Fig. 7b show several differences compared to the 1100 Al results. First, the energy carried away by ejected material was significant, account-

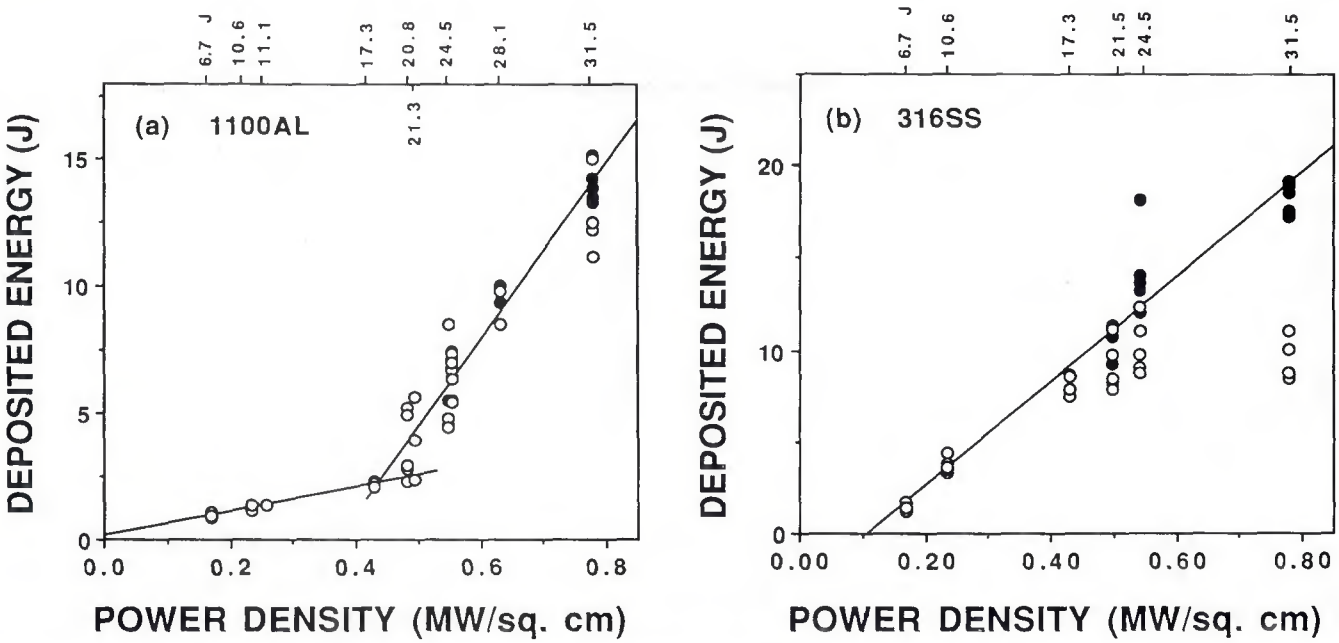

Fig. 7 — Laser pulse energy deposited in a sample as a function of power density incident on sample in argon. a — 1100 Al; b — 316 SS in argon. The data refer to the deposited energy measured by the LVDT (O) and the deposited energy corrected by assuming the ejected material was at the melting temperature (●). The incident pulse energy corresponding to each power density is listed at the top of the graphs.

ing for 50% of the total deposited energy at the highest power density, compared to 10% for 1100 Al. This is due to the greater mass ejected from 316 SS (8-mg average) compared to 1100 Al (1 mg) because the energies required per unit mass to melt the two materials starting from 293 K are within 2%. Second, the data corrected for energy loss by the ejecta can be fit to a single line, that is, there was no threshold power density above which the coupling efficiency increased significantly, as observed for 1100 Al. Third, the fraction of energy deposited was greater for 316 SS at all power densities. The energy deposited at the lowest power density was about 21%, whereas at the highest power energy coupling was about 62%, both values being about a factor of 1.4 greater than measured for 1100 Al at the corresponding power densities. Assuming the ejected mass was at the boiling temperature yields an average energy coupling of 93% for 316 SS.

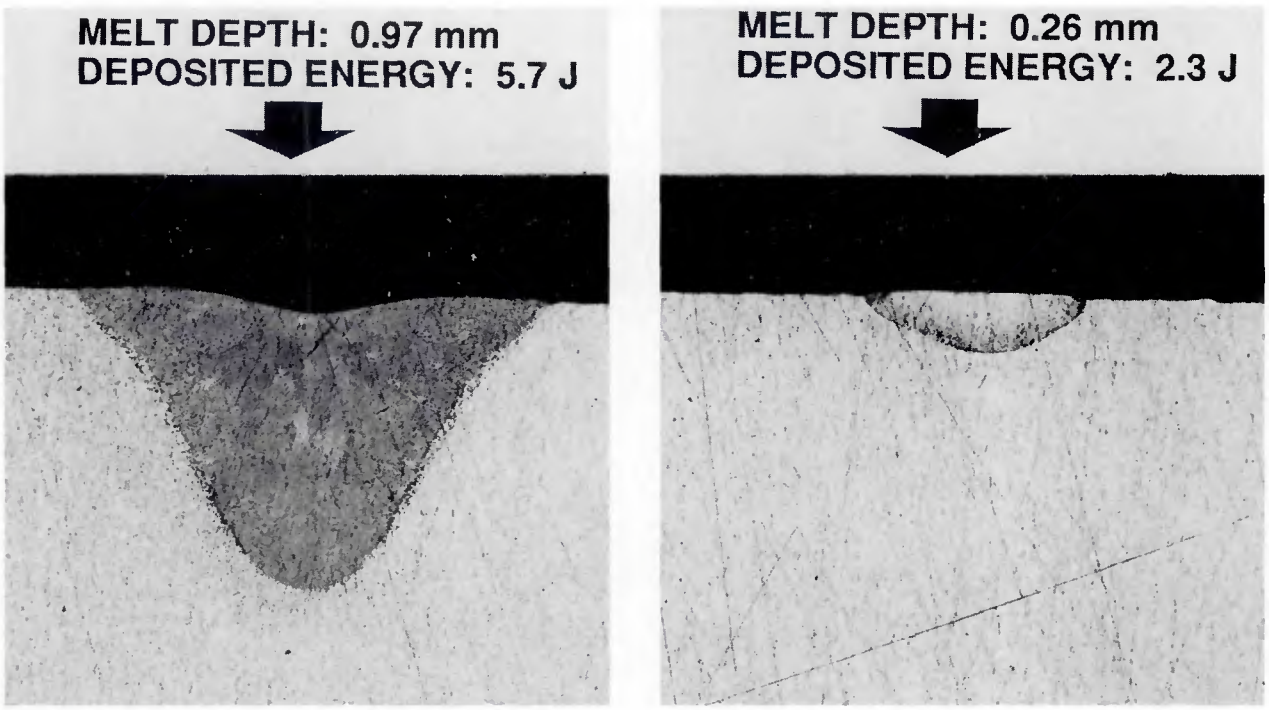

Fig. 8 — Cross-sections of melts made in 1100 Al at power densities of 0.48–0.49 MW/cm² under identical conditions. The melt depth and deposited energy are listed. No material was ejected from the molten pools.

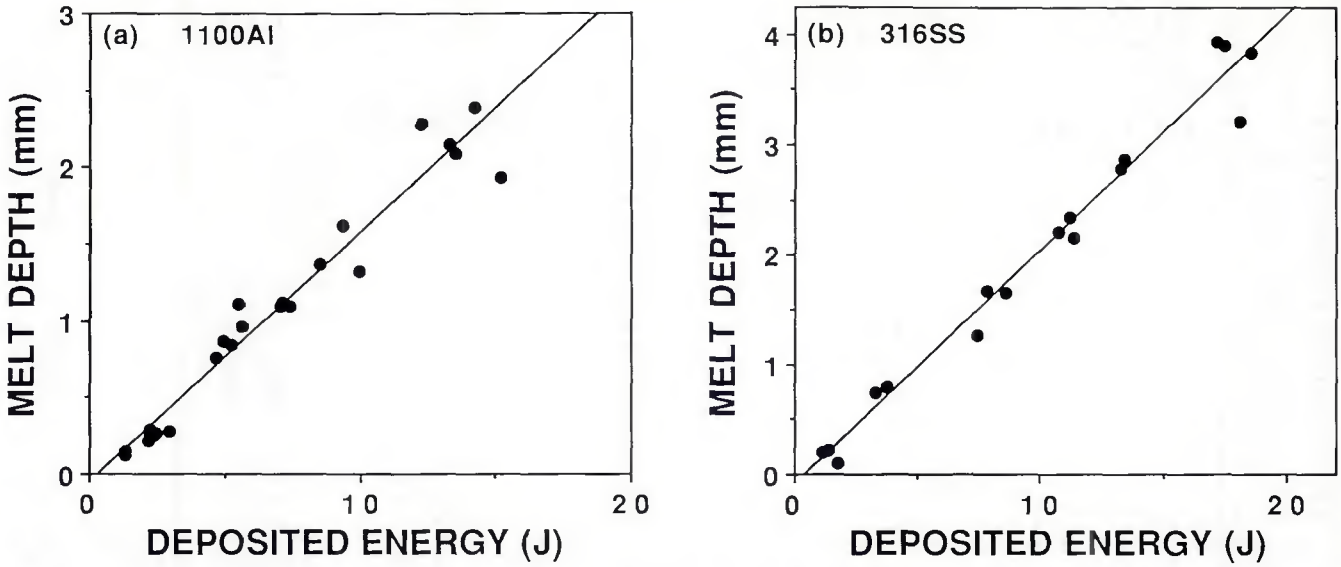

Fig. 9 — Dependence of melt depth on total energy deposited. a — 1100 Al; b — 316 SS. The deposited energy is the sum of the energy measured with the LVDT and the energy removed by ejected material at the melting point.

Melt Depth

Forty-two of the samples corresponding to the data in Fig. 7 were cross-sectioned to determine the maximum melt depth. In Fig. 9, the melt depths are plotted against the total deposited energy for 1100 Al and 316 SS assuming the ejected material was at the melting point. The data show a very good correlation between melt depth and total absorbed energy over the range examined here. Somewhat surprisingly, a correlation was observed even at the highest powers where material was ejected from the melt pool.

Effect of Surface Condition

The condition of the sample surface (*e.g.*, roughness, composition) is known to affect melt depth (Refs. 12–14). The effects of surface condition were demonstrated using the interferometer and samples of 1100 Al and copper. Samples of 1100 Al were prepared having different finishes: machined, semipolished (1–6 micron grit), rough (120 grit), grit-blasted, and black anodized. Copper samples were used with machined surfaces and surfaces anodized with hard coats of ebanol-c having thicknesses of 0.013 and 0.025 cm. The absorption of ebanol-c at 1.06 μm is significantly greater than that of bare copper. For these preliminary experiments no attempt was made to measure surface roughness or reflectivity. The percent of incident laser energy coupled into these materials is listed in Table 2.

The data show that energy coupling increased with increased surface roughness and with the addition of an absorptive coating. In both cases, this can be attributed to decreased surface reflectivity. For example, increasing average roughness from 0.2 to 1.6 μm decreases the reflectivity of a nickel surface from 0.4 to 0.27 for a 50-deg angle of incidence (Ref. 15).

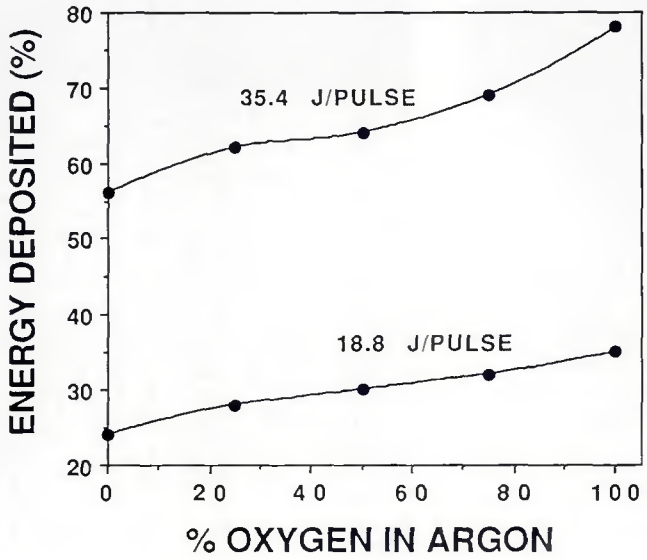

Fig. 10 — Percent energy coupled into 1100 Al as a function of the percent oxygen in argon of the cover gas for two incident laser pulse energies. Measurements made with the interferometer.

Effect of Atmosphere

The atmosphere above the melt is known to change the melt depth (Refs. 12, 16). The effect of oxygen was studied by flowing mixtures of argon and oxygen through the chamber above the 1100 Al samples and measuring the deposited energy with the interferometer. The results are presented in Fig. 10. There was a monotonic increase in deposited energy as the percentage of oxygen in argon increased. The deposited energy was about 40% greater in 100% oxygen, for both pulse energies, than that measured using a 100% argon cover gas. This increased coupling may result from oxygen-induced changes in melt circulation (Ref. 17) or from increased absorption by aluminum oxides at the surface (Ref. 12). Energy could also be evolved in the melt from the highly exothermic reaction $4Al + 3O_2 = 2Al_2O_3$ with $\Delta H = -401$ kcal/mole. For example, to increase the energy deposited from 24 to 34%, which corresponds to an increase in energy of 2.1 J for an incident energy of 18.8 J/pulse, only 63 μg (about 25% of the melt) of aluminum must react with oxygen.

Comparison of Methods

Both the interferometer and the LVDT are useful to measure the transient expansion of a small sample due to laser heating. The advantages of the interferometer are self-calibration and sensitivity. One complete fringe shift corresponds to a change in sample length equal to the He-Ne laser wavelength. In principle, using the Michelson interferometer shown in Fig. 1, it

should be possible to measure displacements on the order of 0.01 of the wavelength of the He-Ne laser. Achieving this sensitivity may be difficult, however, without stabilizing the fringe pattern in some manner against vibrations and thermally-induced drift (Ref. 18). Disadvantages of the interferometer are its apparatus complexity and the fringe shift signal must be analyzed to determine sample expansion.

The main advantages of the LVDT are simplicity, small size, and the direct relationship between the LVDT signal and sample expansion. The main disadvantage is limited sensitivity compared to the interferometer.

Conclusions

Two experimental techniques have been developed to measure the laser energy coupled into a metal by measuring the thermal expansion of the sample after the laser pulse with an interferometer or an LVDT. The absorbed laser energy was found to be directly proportional to the melt depth for incident pulse energies from 6.7 to 31.5 J in both the conduction and keyhole welding mode for 1100 Al and 316 SS. A correlation was found even if material was ejected from the melt by assuming the ejected material was at the melting point. Therefore, measurements of the deposited laser energy using these two devices can provide a quick and efficient evaluation of the effects of laser parameters, atmosphere, alloy composition, and surface condition on the resulting melt depth compared to tedious and time-consuming metallographic cross-sectioning.

Acknowledgments

This work was done under the auspices of the U.S. Department of Energy. The authors appreciate the funding given this work by the Laboratory Directed Research and Development program at Los Alamos National Laboratory.

References

1. Arata, Y. 1986. *Plasma, Electron and Laser Beam Technology.* ASM International, Materials Park, Ohio.

2. Touloukian, Y. S., Kirby, R. K., Taylor, R. E., and Desai, P. D. 1977. *Thermal Expansion, Metallic Elements and Alloys: Vol. 12.* IFI/Plenum. New York, N.Y.

3. Lim, G. C., and Steen, W. M. 1984. Instrument for instantaneous *in situ* analysis of the mode structure of a high power laser beam. *J. Phys. E: Sci. Instrum.* 17:999 to 1007.

4. *Metals Handbook 9th ed.: Vol. 2.* 1979. ASM International, Materials Park, Ohio.

5. Touloukian, Y. S. (ed.) 1967. *Thermophysical Properties of High Temperature Materials Vol. 3.* Macmillan Co., New York, N.Y.

6. ABAQUS Version 4.8, Copyright 1990, Hibbitt, Karlsson, and Sorenson, Inc., Providence, R.I.

7. Chun, M. K., and Rose, K. 1970. Interaction of high-intensity laser beams with metals. *J. Appl. Phys.* 41:614 to 620.

8. Dixon, R. D., and Lewis, G. K. 1985. Effect of angle of incidence on plasmas generated during laser welding. *Proc. of the 1984 ICALEO.* Boston, Mass.

9. Bonch-Bruevich, A. M., Imas, Ya. A., Romanov, G. S., Libenson, M. N., and Mal'tsev. 1969. Effect of a laser pulse on the reflecting power of a metal. *Sov. Phys.-Tech. Phys.* 13:640 to 643. (1968. *Zh. Tekh. Fiz.* 38:851 to 855).

10. Basov, N. G., Boiko, V. A., Krokhin, O. N., Semenov, O. G., and Sklizkov. 1969. Reduction of reflection coefficient for intense laser radiation on solid surfaces. *Sov. Phys.-Tech. Phys.* 13:1581 to 1582. (1968. *Zh. Tekh. Fiz.* 38:1973 to 1975).

11. Banas, C. 1986. High power laser welding. *The Industrial Laser Annual Handbook 1986: Sec. II.* PennWell Books, Tulsa, Okla.

12. Jorgenson, M. 1980. Increasing energy absorption in laser welding. *Metal Construction* 12:88.

13. Bashenko, V. V., Gol'tsova, V. P., and Batkin, E. S. 1979. The effects of the roughness of metal on the depth of penetration in pulsed laser welding. *Avt. Svarka.* No. 5: 41 to 42.

14. Ursu, I., Mihailescu, I. N., Popa, Al., Prokhorov, A. M., Konov, V. I., Ageev, V. P., and Tokarev, V. N. 1984. CO_2-laser radiation absorption by metal gratings. *Appl. Phys. Lett.* 45(4):365 to 367.

15. Peiponen, K.-E., and Tsuboi, T. 1990. Metal surface roughness and optical reflectance. *Optics and Laser Technology* 22(2):127 to 130.

16. Davydov, V. A., and Magnitskii, O. A. 1982. Formation of the surface of the weld spot in laser welding. *Svar. Proiz.* No. 12: 20 to 21.

17. Heiple, C. R., and Burgardt, P. 1985. Effects of SO_2 shielding gas additions on GTA weld shape. *Welding Journal* 64(6):159-s to 162-s.

18. Cremers, D. A., and Keller, R. A. 1982. Thermooptic-based differential measurements of weak solute absorptions with an interferometer. *Appl. Opt.* 21:1654 to 1662.

WRC Bulletin 360
January 1991

Stress Indices, Pressure Design and Stress Intensification Factors for Laterals in Piping

By E. C. Rodabaugh

The study described in this report was initiated in 1987 by the PVRC Design Division Committee on Piping, Pumps and Valves, under a grant to E. C. Rodabaugh following an informal request from the ASME Boiler and Pressure Vessel Committee, Working Group on Piping (WGPD (SGD) (SC-II) to develop stress indices and stress intensification factors (*i*-factors) for piping system laterals that could be considered by the ASME committee for incorporation into the Code.

In this study, E. C. Rodabaugh considered all available information on lateral connections in concert with existing design guidance for 90-deg branch connections; and has developed compatible design guidance for lateral connections for piping system design. As a corollary bonus, he has also extended the parameter range for the "B" stress indices for 90-deg branch connections from d/D = 0.5 (the present Code limit) to d/D = 1.0. Therefore, this report should be of significant interest to the B31 industrial piping code committees, as well as the ASME Boiler and Pressure Vessel Committee.

Publication of this report was sponsored by the Committee on Piping, Pumps and Valves of the Design Division of the Pressure Vessel Research Council. The price of WRC Bulletin 360 is $30.00 per copy, plus $5.00 for U.S. or $10.00 for overseas postage and handling. Orders should be sent with payment to the Welding Research Council, 345 E. 47th St., Room 1301, New York, NY 10017.